

A Study on the Dynamic Characterization of a Tunable Magneto-Rheological Fluid-

Elastic Mount in Squeeze Mode Vibration

By

Akram Anwar

Chapter 1 | Introduction

This first chapter serves as a brief overview and guide to the remainder of the thesis. It begins by providing a background section featuring the history of vibration isolation and vibration absorbers and their uses in current applications. It then turns the discussion to magneto-rheological fluids and their potential uses in tunable vibration absorbers. Next, a section is presented that lists the deliverable objectives of this research study and the driving factors that inspired the pursuit of these goals. The approach section discusses the method by which the objectives are achieved. An outline section lays out the organization of the chapters in this document. And finally, a contributions section highlights what contributions this work will be making to the field of tuned vibration absorber development.

1.1 | Background

Since moving machines were first invented, the suppression of unwanted vibrations has been a lingering problem. Whether it is found in state of the art manufacturing equipment, supersonic aircraft or the most commonly driven car on the road, there always exist input vibrations. These vibrations, though seemingly harmless, can lead to machine misalignment, operator fatigue and could significantly reduce the quality and ultimately the usable lifetime of the equipment. Therefore, certain devices have been extensively developed and their usefulness has been studied. Of these devices, are vibration-isolating mounting platforms, simply known as mounts. Initially, these platforms were made of an elastomer that could be tuned for a range of frequencies [1]. However as technology evolved, the mounts also evolved into fluid filled hydraulic elastomeric mounts capable of isolating a vastly greater bandwidth of frequencies. However, due to the nature of these passive mounts, they are generally unable to account for start-up modes from a rotating motor or vehicle engine because they are designed to conquer vibrations that occur at the devices' operating ranges, which generally falls between 10 - 100 Hz. Additionally, the threshold for human perception of vibrations is between 1 - 10 Hz making suppression in this range all the more important because humans can perceive these frequencies the most [2].

The second category of mounts that were mentioned, the fluid filled or hydraulic mounts, can provide better performance at natural frequencies and resonance modes [1]. Included in those frequencies are those that an engine or equipment would encounter at both start-up as well as normal operating speeds. To further improve on the concept, there have been studies on hydraulic mounts featuring smart materials. [2]. Of these materials are Magneto-Rheological (MR) Fluids. MR-Fluids were first invented in the early 1940's by Jacob Rabinow [3] and are now some of the best known and most widely researched smart fluids in tunable suspensions [4]. MR-Fluids consist of micron-sized Ferro-magnetic particles dispersed in a non-magnetic oil-based carrier fluid, generally mineral or synthetic oil, water or glycol [5]. Because of this, the fluid acts as a normal free flowing suspension fluid when not magnetized. However, its rheological behavior changes when a magnetic field is applied [6]. This is advantageous because the mix of Ferro-magnetic particles and carrier fluid, can easily switch from Newtonian-like fluid behavior to the behavior of a stiff semi-solid by applying a magnetic field of 0.1-0.5 Tesla [6]. Because of their versatile nature, MR fluids are currently being used in a variety of other applications including controllable dampers, rotary brakes [7] and even in prosthetic devices [8] and earthquake suppression in buildings [9].

Mounts and electromagnetic mount assemblies that feature MR Fluids have been designed and tested before, such as in the studies conducted by Wang et al. and York et al., both detailed in the background chapter of this document. However, the driving point behind this study is to continue the research first initiated by BM Southern. In that study, the main purpose listed was to design a slender elastomeric MR-Fluid mount with an efficient and low profile magnetic activation system [10]. That study however, only went as far as developing the mounts and determining their characteristics. In order to validate, determine the efficiency and dynamic range, as well as to determine overall usability of the mount configuration, a set of dynamic tests were completed. The results from which will be detailed in this study.

1.2 | Objectives

The primary objectives of this research study are to:

1. Better understand the dynamic characteristics of a special class of hydraulic mounts that use MR fluid
2. Determine the factors that influence dynamic isolation properties of the MR mounts
3. Conduct experiments that allow us to quantify the dynamic isolation improvements of the MR mounts
4. Provide recommendations for future studies that can help with the practical implementation of the MR mounts

1.3 | Approach

In order to complete the objectives above, we chose the approach of building a test set-up, testing for viability, iterating and re-testing various configurations with the mount designs. Specifically, we will perform the following:

- Evaluate the desired deliverables of the experiment
- Design a custom test set up that is conducive to quasi-static and dynamic testing of the selected MR mounts
- Conduct experimental tests using the custom testing set-up to determine dynamic properties of the MR mounts
- Analyze and evaluate results
- Draw conclusions

1.4 | Outline

The next chapter, Chapter 5, gives a brief overview of MR fluid and its history and current application. It then gives a comparison of existing Tuned Vibration Absorbers (TVA's) that are passive with the ones that feature the MR fluid technology. Chapter 6 presents the design of the experiment conducted in this research study. It specifically covers the test set-up, the form of data acquisition and finally the validation of these systems. In Chapter 7, the results of the dynamic test are presented in extensive detail. It then shows the mathematical model developed and compares it to the results attained. Finally, Chapter 8 presents the concluding remarks as well as potential research possibilities for future work with this design.

1.5 | Contributions

The main motivations of this research are to contribute to the existing technologies and to build upon the successes of the research of others within the field of TVA and MR fluid-elastomeric device development. The main contributions of this research include providing a better understanding of the dynamic isolation properties of a special class of MR mount that can be used for a variety of industrial applications. Also a part of the contributions of this research will be to quantify the amount of dynamic isolation that is observed through these mounts and to compare it with conventional passive mounts of the same configuration. This is the first study of its kind for this design of squeeze mode MR mounts.

Chapter 2 | Background and Literature Review

This chapter provides the scientific and engineering background information necessary to understand the reasoning behind the steps taken in the design and execution of this study. This chapter begins by providing a history of MR technology, from its origins to its many available forms today. Next a section is presented on previous work in fluid mounts and MR mounts, including the predecessors to the ones designed in this study. Lastly, a brief discussion on useful dynamics and vibrations analysis techniques is presented.

2.1 | MR Fluid History and Background

2.1.1 MR fluid history and physical composition

Jacob Rabinow was credited with being the first to invent MR fluids in 1948 [1]. He observed that certain materials would thicken and become solid when exposed to a magnetic field.

Rabinow eventually patented his findings in “Magnetic Fluid Force and Torque Transmitting Device” [2]. Since then, the technology has evolved immensely. Despite the evolutions, the basic make up of MR fluids has pretty much remained the same. MR fluids are generally made up of three components: ferromagnetic particles, a carrier fluid, and a stabilizer.

The ferromagnetic particles are generally made of Iron or Iron-based magnetosoft materials. [3, 4, 5]. More specifically, these particles are typically of carbonyl iron and are usually spherical in shape. However, Iron alloy particles, including iron-nickel and iron-cobalt alloys, are found to perform much better than the original carbonyl iron. The particles sizes are preferred to be between 1 and 10 although successful usage of particles as small as 0.1 and as large as 100 has been reported [3]. These alloys tend to cost much more than the iron carbonyl and thus are not as commonly used. These particles are limited to between 20% and 40% to allow the fluid to retain its flowing fluid-like properties [6, 7].

Secondly, there exists a carrier fluid in which these ferromagnetic particles are suspended. This carrier fluid acts as a continuous isolating medium and is generally made of silicon oil, kerosene, mineral oil, or a mixture of water and glycol [4, 8, and 9]. The selection criteria that the fluid must meet are simple. It should have a low initial viscosity, good anti-corrosion properties and a

wide range of temperature stability. A viscosity of at an ambient temperature of is ideal for correct operation [14].

Lastly, in this mixture of particles and carrier fluid, a stabilizer is added. The stability of the fluid determines the lifetime and the durability of it. And thus, the stabilizer is another important part of the overall make up. [14].



Figure 2-1

: A container of Lord Corp MRF-122 that has separated into carrier fluid and material sediment.

Although this study focuses only on devices that use MR fluids, it is important to note that almost concurrently with the discovery of MR fluid by Rabinow, Winslow had discovered electro-rheological (ER) fluids [19, 20]. ER fluids are electrically polarizable particles suspended in an oil that is electrically insulating along with cornstarch, silica, barium titanate or other semiconductors [21]. These fluids have properties that are similar to MR fluids. However, the viscosity of ER fluids changes when an electric field was applied to the material.

2.1.2 Magnetorheology

In the off state, MR fluid acts like any other fluid. Essentially, it is comparable to a higher viscosity version of the carrier fluid due to the added density of the suspended particles, (at low shear rates) [14]. The viscosity has the ability to change $\sim 10^2$ times, within 10 ms in some cases, upon magnetic field application. Additionally, when the field is removed, the effects are completely reversed [22, 26, 27]. When the field is present, the fluid

acts as a toothpaste-like Bingham plastic flowing material [10]. The change in properties of the fluid is studied and characterized through a series of yield stress tests through various magnetic field intensities at high velocity and high shear rates [11].

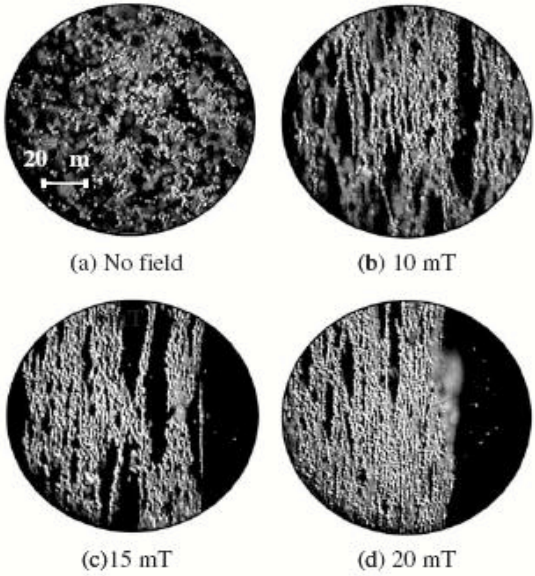


Figure 2-2: Polarization and alignment of ferrous iron in MR fluid, adapted from Ahn et al. [12].

This change in viscosity, and subsequently yield stress, is due to the ferromagnetic particles forming chains in the fluid when a magnetic field is present [13, 14]. As can be seen in figure 2-2 above, as the magnetic field is applied with increasing magnitude, the chains become more and more evident [15]. The strength of these chains is also dependent on the intensity of the magnetic field. These chains can only be broken when the necessary amount of shear stress is present; this value is known as the yield stress of the magnetic chain structures [16].

2.1.3 MR Fluid Modes of operation

MR fluids can be operated in 3 modes: Valve mode, Direct Shear mode, and Squeeze mode. The most popular mode of operation for MR fluids is currently Valve mode, also known as pressure driven mode by Lord Materials Division. The basic premise behind valve mode operation is that the fluid’s controllable viscosity determines how quickly the fluid passes through a damper or valve. The flow is directed perpendicularly between two magnetic pole plates [17]. This can be seen in figure 2-3 below showing the flow of the fluid through the chains of suspended material. The amount of magnetic field varies the viscosity, thus dictating the amount of energy dissipated by a shock absorber employing MR fluid.

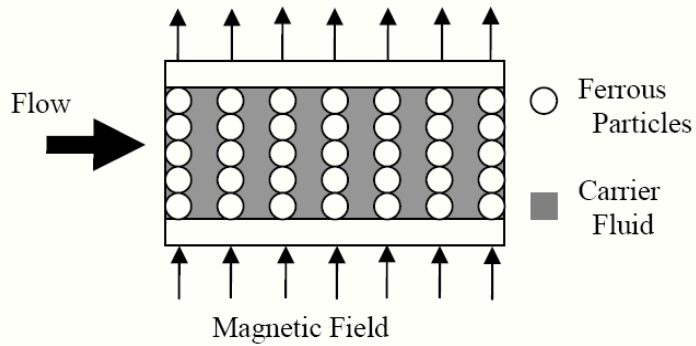


Figure 2-3: MR fluid in valve mode with an applied magnetic field, adapted from [22]

The next, more well-known, operation mode for MR fluid is in direct shear mode. In this mode, the relative motion between the magnetic pole plates perpendicular to the magnetic field flow is hindered by the particle chains' tendency to remain together. Without a magnetic field, the two pole plates act with the normal amount of resistance that a fluid with the MR's inactive fluid viscosity would provide. However, when the magnetic field is applied, the chains appear in the fluid thus adding an increased shear force. This is shown below in figure 2-4.

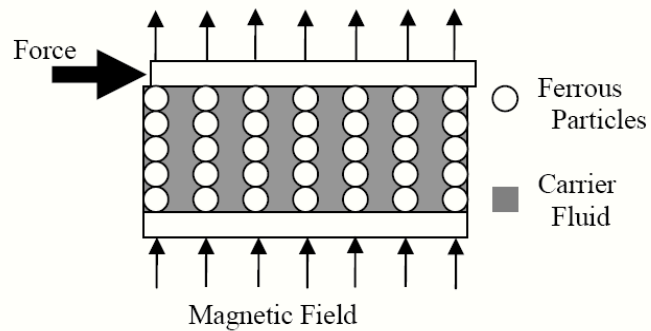


Figure 2-4: MR fluid in shear mode with an applied magnetic field, adapted from [22].

Lastly, the most relevant mode to this study is the squeeze mode operation. The squeeze mode utilizes the analogy of a buckling columnar structure. In this mode, the lateral force applied is parallel to the magnetic field lines [22, 23]. This mode is used primarily for operational modes that require high stiffness and low displacements. The MR fluid may also be embedded in a cavity within another material that provides passive stiffness and damping characteristics when the fluid is not activated. When activated, the axial force applied is resisted by the chains of suspended material and the fluid offers variable axial compressive strength [23]. The figure below shows the squeeze mode before and after application of axial force. Note the resistance of the particle chains.

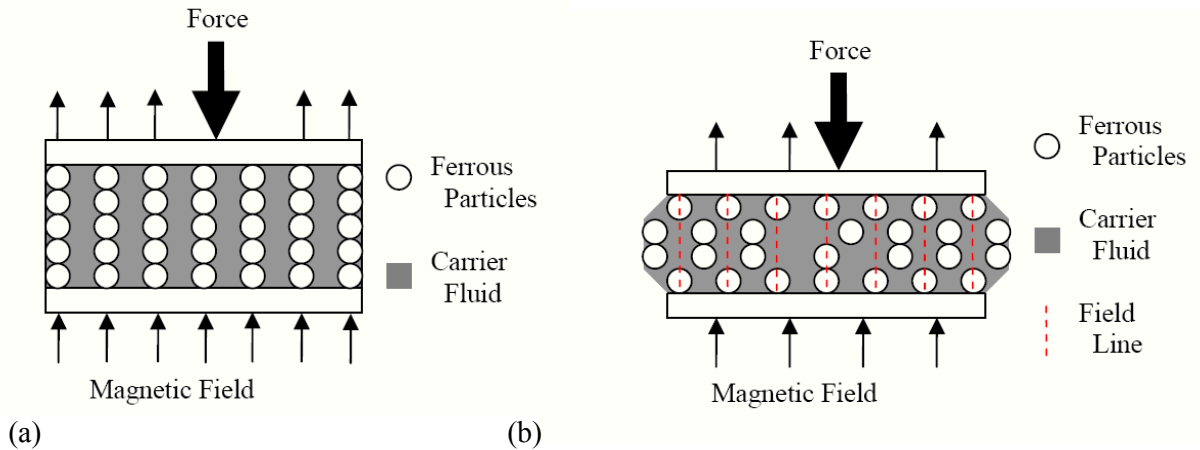


Figure 2-5: MR fluid (a) in squeeze mode setup prior to axial force with an applied magnetic field, and (b) squeeze mode operation with axial force and applied magnetic field, adapted from [27].

As the force is applied and the chains begin to compress, the chains begin to aggregate as is shown in figure 2-6 below adapted from Goncalves et al. [29]. This aggregation adds a certain amount of compressive strength when loaded but does not present itself when loading is inexistent. This tends to cause hysteresis in the unloading portion of a loading cycle as was discovered by York et al. as well as BM Southern [11, 30].

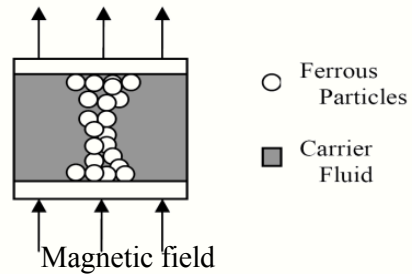


Figure 2-6: Ferrous particle aggregation in squeeze mode operation after experiencing a compressive load, adapted from [29].

2.1.4 The Advantages of MR Fluids

The use of MR fluids is advantageous in many different respects. Firstly, the reaction time of the particles upon the application of a magnetic field is in the milli-seconds. However, in order to fully utilize this aspect, one must have an electromagnet that will react quicker than the fluid itself [7]. Next, the material is controllable and very compliant. As long as it is stable, the material will invariably return the same result, repeatedly. The material's change in viscosity is also completely reversible with no sign of artifacts or material memory [14]. The magnetic field required is in the mTesla range, and the power required to apply that amount is minimal [7].

Another advantage is the fluid's stability through a range of temperatures. This robustness to change in temperature as well as its lack of history dependency was tested and confirmed through various research studies. Tests on temperature robustness were conducted by Weiss and Ducloss, tests on magnitude of magnetic field vs. power supply were conducted by Tang and Conrad and tests on history dependency as well as the stability of the carrier were conducted by Ashour, Rogers et al. [21, 22, 14].

Table 2-1: General properties of MR Fluids, adapted from [4].

Specification	Remark
High Dynamic Yield Strength	Instantaneous generation of from 0 to 90 Pa yield stress for precise real-time control
Wide Operating Temperature Range	-40° to 150° with less than 10% variation in maximum dynamic stress
Millisecond Response Time	Ideal for use in applications requiring continuously variable, high-precision control
Non-Abrasiveness	Additives in MR fluids reduce abrasiveness, enabling devices to achieve required life expectancies
Low Sedimentation Level	The formulation of MR fluids solves sedimentation and stratification problems found in other MR fluids
Current Density	Can energize with permanent magnets
Specific Gravity	2-4
Ancillary Materials	Iron/Steel
Color	Black/Grey

2.1.6 MR Fluid Device Applications

Because of its versatile nature and many modes of operation, there exist many applications of MR Fluids. Although, many of these applications can be found in the automotive industry, there are also many applications outside of the automotive realm that benefit from MR technology. These applications include adjustable dampers, rotary clutches and brakes, seismic vibration mitigation devices and even prosthetic devices [4, 9, 10]. MR fluids are now gaining notoriety as many automotive manufactures are offering MR fluid operated semi-active suspension systems such as Chevrolet’s Magnetic Selective Ride Control (MSRC) available on the Corvette, Camaro and Cadillac CTS-V [33]. Future roles that MR fluids may be pivotal in include power transmission systems, aeronautical servo systems, structure vibration control, optical grinding, MEMS, and robotic systems [34-39].

2.2 | Passive and Active mount history

2.2.1 Passive Mounts: Fluid-Elastic Mounts

This section describes a few examples of recent developments in passive mounts. Of these mounts, only the fluid filled or hydraulic mounts are described in detail in this section to show the contrast between a passive fluid filled mount and an active or semi-active mount. A hydraulic mount, as is seen below in figure 2-9, consists of two chambers and a decoupler. Fluid inside of the mount travels from one chamber to the other and encounters resistance from having to find a flow path through the inertial track. Additionally, a pressure differential causes the decoupler to move depending on whether the mount is experiencing compression or extension. The amplitude of the motion also affects the extent of movement and deflection that the coupler will experience [21]. Christophereson et al. rationalized the mathematical model for this simple hydraulic mount and the force being transmitted [22].

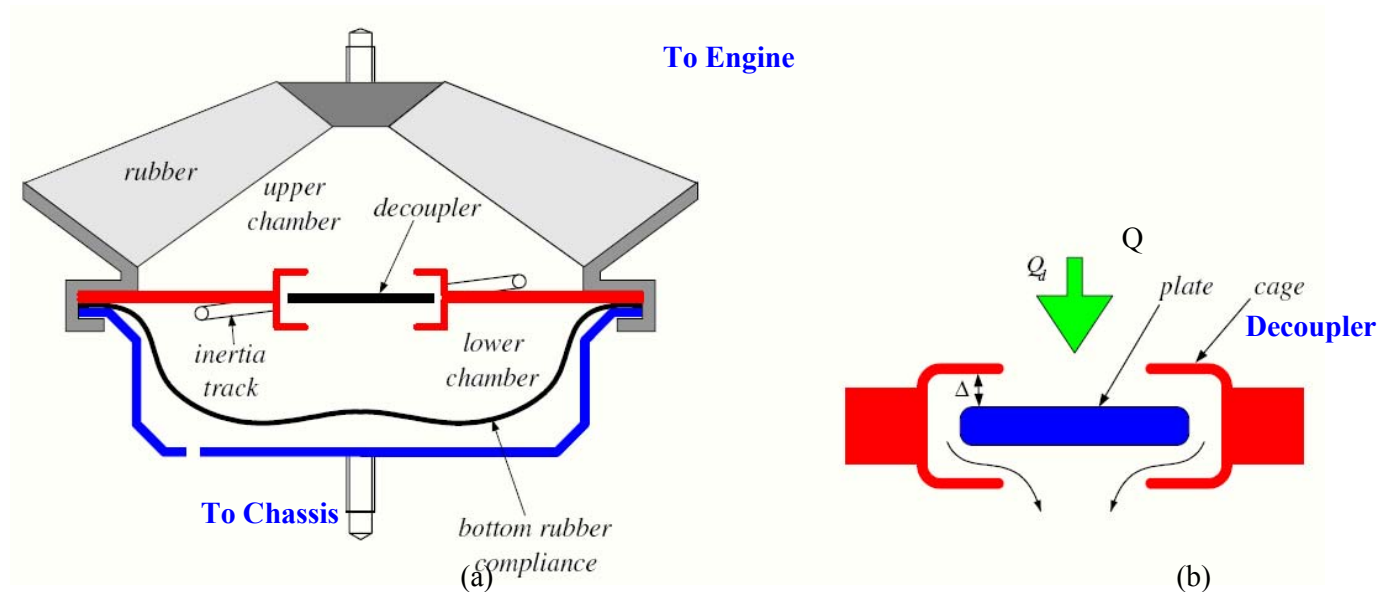


Figure 2-9: Two chamber passive hydraulic fluid mount with decoupler, adapted from [22].

Unfortunately however, as was described in earlier sections, passive mounts are rarely able to attenuate all of the input vibrations in a system. Rather, they are tuned for the operating point of the system and do not account for startup modes. Passive hydraulic mounts however, pose a secondary issue in that the fluid in the chamber must be monitored and may require costly re-tuning at some point in its operating life [23]. Regardless, they still provide excellent vibration isolation for many applications.

2.2.2 Active Mounts: MR Fluid-Elastic Mounts

The last and most important type of active mount are a combination MR Fluid-Elastomeric mount. The mounts investigated and characterized in this study are of this type. MR Fluid-Elastic Mounts are defined as mounts with an elastomeric casing as well a fluid cavity to accommodate MR Fluid. Thus far, not many designs exist, but a few of the ones that do are detailed in this section. Wang et al. showed much promise with their initial design. This design places a fluid-elastic mount in between an upper magnetic pole and a lower magnetic shield. With this setup, the mount is operated in the squeeze mode, showing a 40% increase in output force while magnetized; the mount is shown in figure 2-9 below [44].

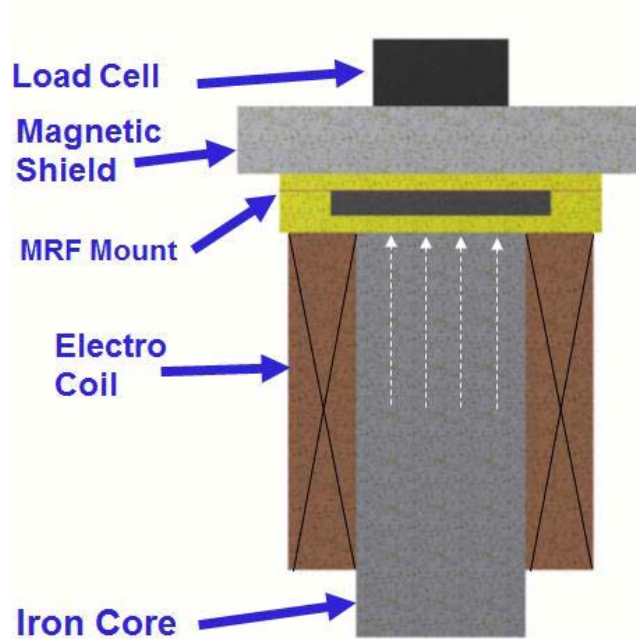


Figure 2-9: Original mount and electromagnet design as proposed by Wang et al. , adapted from [44].

The magnetic set-up by York et al. builds on the design by Wang et al. but requires that the poles be placed directly above the fluid cavity. Although this would drastically increase the effectiveness of the mount, it also requires a large magnetic field generator and bulky packaging [30].

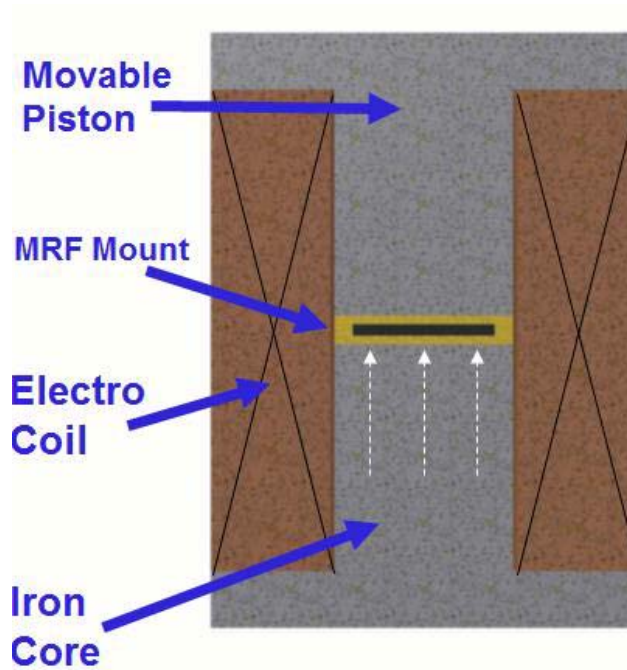


Figure 2-10: Mount and electromagnet design by York et al. , adapted from[30].

Lastly, BM Southern built upon both the design of the elastomeric casing design by Wang et al. as well as the electromagnetic enclosure by York et al. [30, 31]. By adding upper and lower pole plates, the improved design channels the magnetic flux through the center of the mount and the directly into the MR fluid cavity using a funneled upper and lower pole plate configuration. The flux path was analyzed using Finite Element Magnetic Modeling (FEMM) Software to determine the flux path and density. This was all done while making the packaging less than half the height and making the diameter slightly smaller. This new design is called an MR Metal-elastic mount [31].

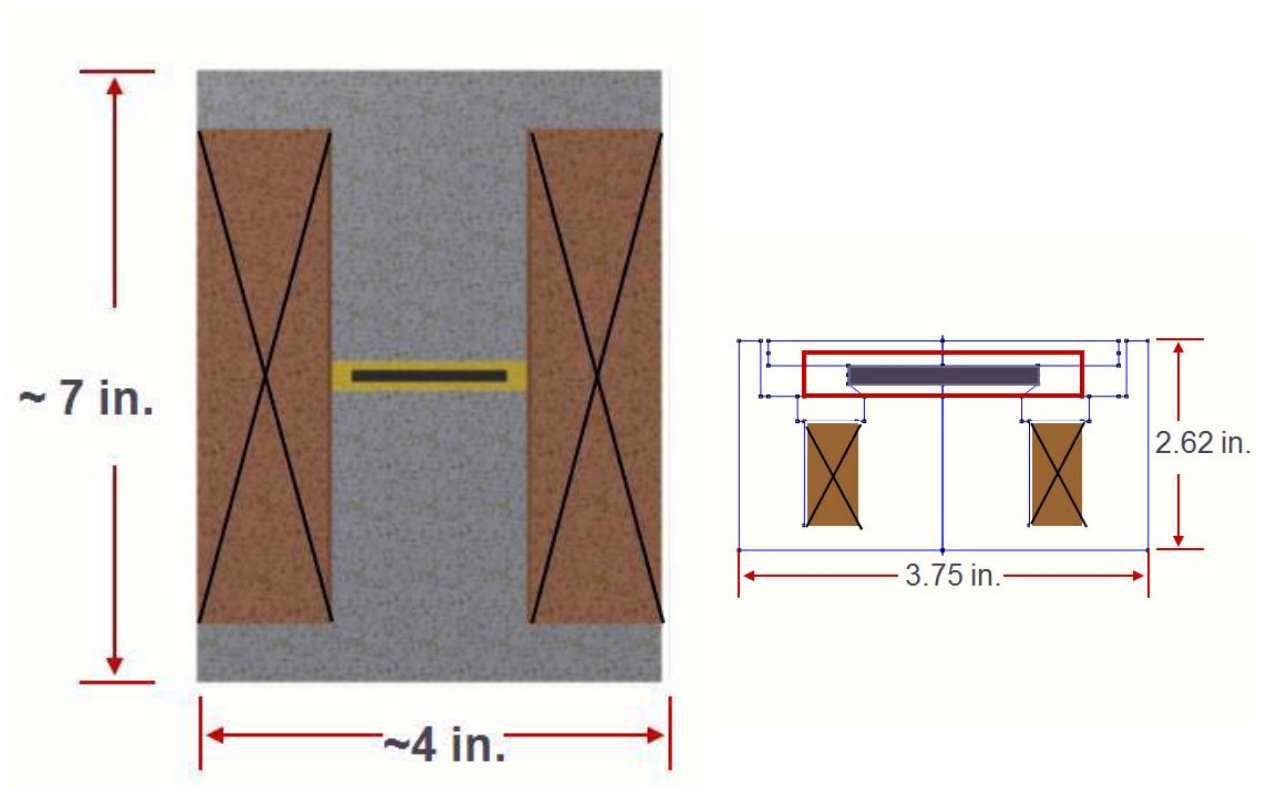


Figure 2-11:

Comparison of previous design (left) with improved design used for this study (right), adapted from [30, 31].

The results of that research study, utilizing the modified lower profile design, showed that at the maximum magnetic field, the mount experienced up to 44% stiffness increase and up to 20.0% damping increase, while only using a maximum of 2 amps of current [31]. This makes it a great candidate for further dynamic characterization and for possible implementation in industrial applications.

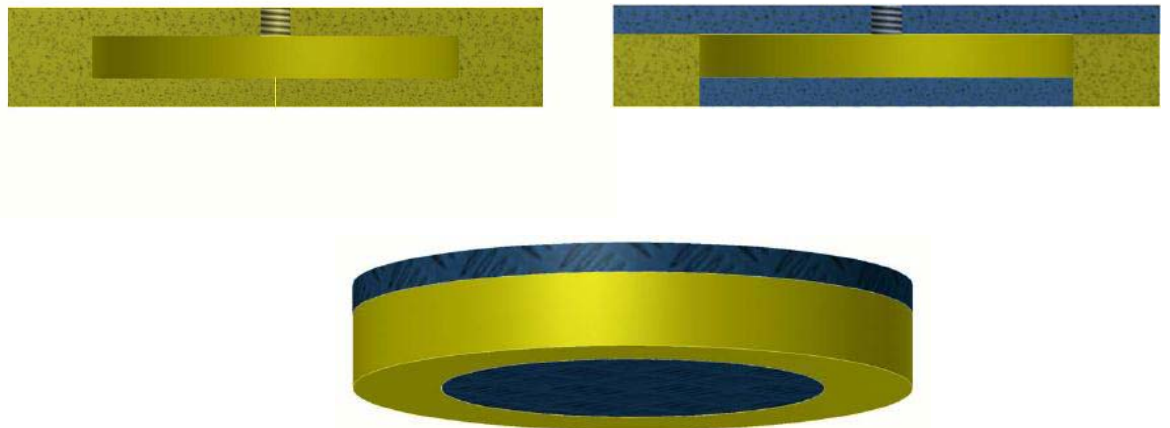


Figure 2-12: Elastic Casing sectional view (top left), Elastic Casing with magnetic-pole plate inserts sectional view (top right), and isometric view of metal-elastic casing (bottom), adapted from [31].

2.2.3 Active mounts: Other MR Mounts

Many active MR mounts have been designed that act like hydraulic mounts or dampers. Employing pistons or chambers, they operate in squeeze mode but pose as a sort of hybrid design. Those designed by Ahn et al., Vahdati, and Choi et al. show different methods of providing stiffness and damping through various methods of fluid chamber exchange as well as magnetic field actuation [24, 26, 28]. Ahn et al. show a magnetic core with a chamber of MR fluid that is compressed by a piston [24]. Vahdati describes a small inertial track for the MR reservoir to travel through from upper to lower chamber [26].

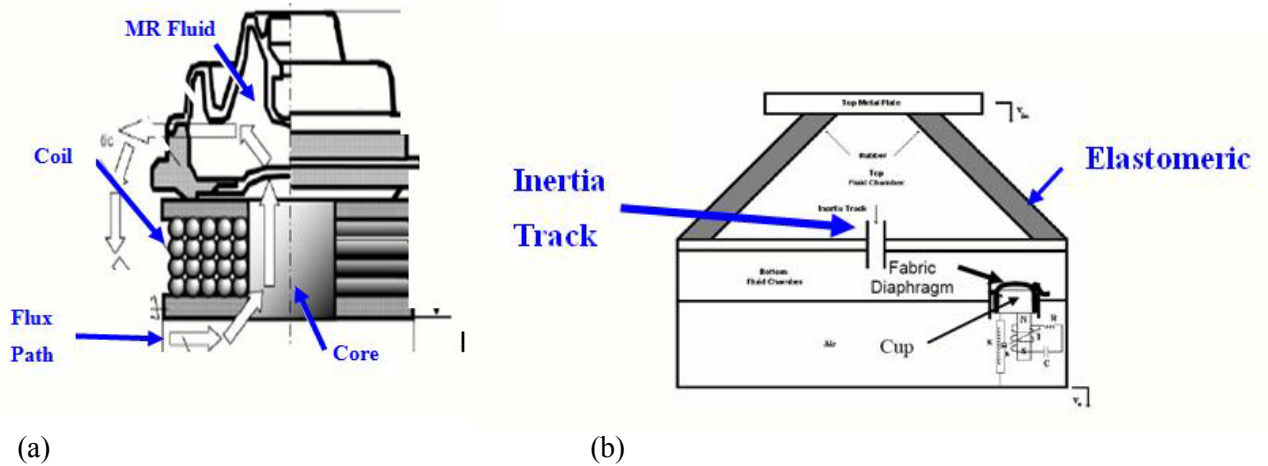


Figure 2-13:

Single chamber MR fluid mount (a), adapted from Ahn et al. [24] and Single pumper semi-active mount (b) proposed by Vahdati, adapted from [26].

Lastly, Choi et al. present a design that features a piston travelling through a reservoir of MR fluid experiencing different levels of resistance with varying magnetic field densities [28].

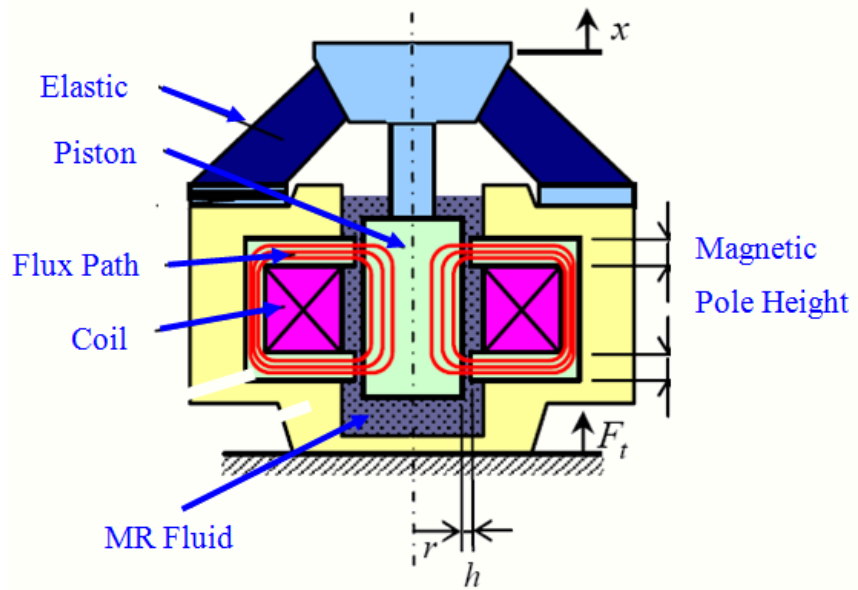


Figure 2-14: MR fluid mount by Choi et al., adapted from [20].

There also exist mount similar in operation to the fluid elastic and metal elastic mounts described above. However, instead of packaging the mount and the electromagnet separately, they share designs with the hydraulic MR mounts in that they are encapsulated in one package, but still operate in the squeeze mode [25]. All of these encapsulated designs do not feature easy MR fluid interchangeability.

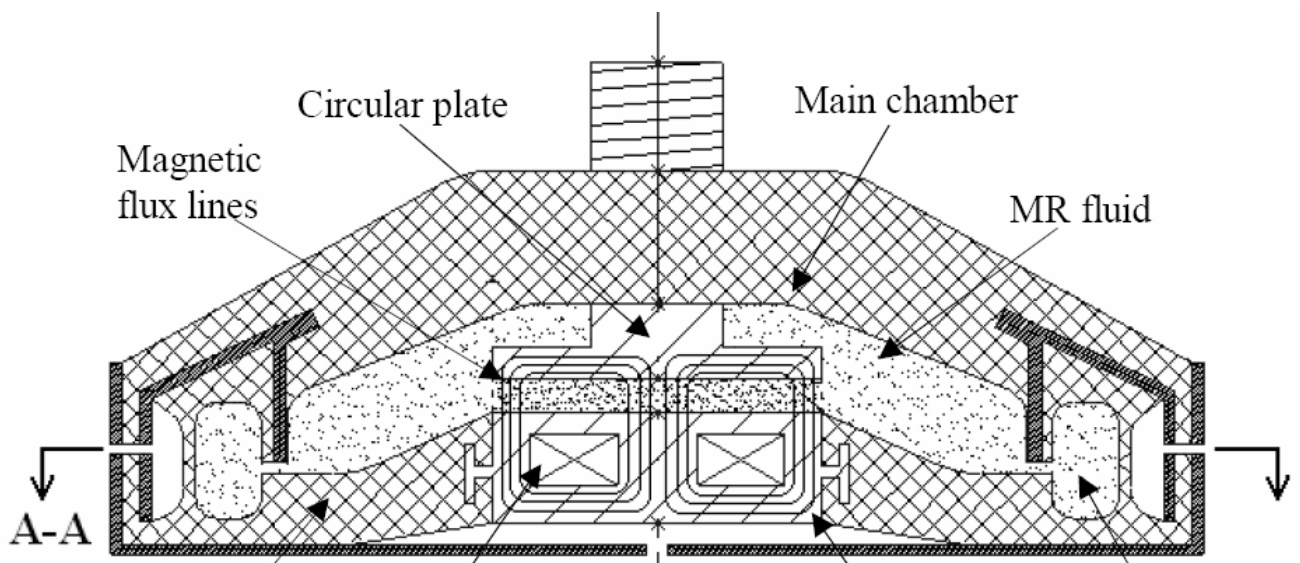


Figure 2-15: Squeeze flow mode MR fluid mount by Nguyen et al., adapted from [25].

۲.۳ | Principles of Vibrational Systems

۲.۳.۱ Basic Model for squeeze-mode mounts

In order to understand the basis behind this study and the format of the test setup, some basic principles of dynamics and vibrations needed to be reviewed and understood. The problem presented in this study is a simple base excited single degree of freedom (SDOF) system problem and can be modeled as a second order differential equation.

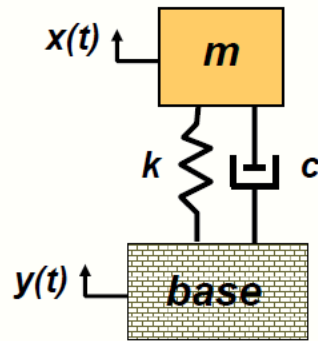


Figure ۲-۱۶: Equivalent mechanical system represented by a spring-mass damper system and a moving base [۳]

In this form, equation ۲.۳ shows the dynamics of the system modeled in terms of stiffness, k , damping, c , and as well as base input displacement, $y(t)$, and relative upper mass displacement, $x(t)$. With a mount, both the spring and damper elements are combined into one package; however both are still quantified separately as they change somewhat independently of each other.

۲.۳.۲ Quasi-Static Characterization

As was described in the objectives section of the first chapter, the main goal is to determine the mounts' abilities to suppress the magnitude of the output vibration at their respective resonance frequencies over a range of magnetic field magnitudes. As will also be seen in later chapters, the natural frequency calculation goes into data validation as well modeling.

In order to determine the natural frequency of any spring mass system, one must use the basic law more involved. Using the hysteretic force displacement curve along with line and area fitting techniques, the equivalent stiffness of the mounts can be determined [29].

where determining the natural frequency, ω_n , requires finding the stiffness of the spring involved and the amount of mass that the test setup has placed on it. Finding the spring constant, k_s , can be done multiple ways. The simplest is to use hook's law which states $F = k_s \delta$ or

Where F is the load force on the spring and δ is its displacement [29]. This is most conveniently done by conducting a quasi-static test (QST). A typical force-displacement QST curve is shown below in figure 2-18 with the non-linear region ignored and spring rate determined using the fit line of the linear portion of the compression and extension plot. This linear relationship is

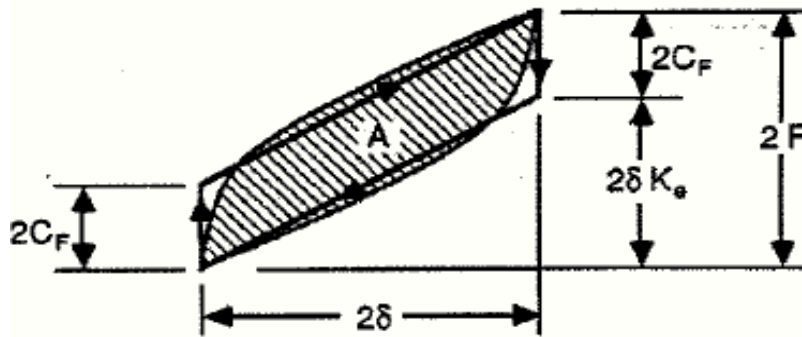


Figure 2-18: Example force-displacement curve showing method of calculation for materials applicable for a mount or spring that acts linearly. For MR mounts in squeeze mode, there exists with hysteretic content [29].

aggregation of MR material chains and thus hysteretic content must be included

The second parameter that is determined from the QST is the equivalent damping of the system.

Inman defines equivalent damping, c_e and damping ratio as follows:

The damping is calculated using the energy dissipated, W_d , as well as the QST displacement, δ ,

test frequency, ω , and the natural frequency, ω_n . The dissipated energy can either be found

graphically by determining the area within the hysteretic loop [29] or analytically by multiplying

and the QST displacement by the hysteretic damping constant, H .

This process was completed extensively and is detailed thoroughly in BM Southern's

dissertation. However, since a significant amount of time had elapsed between the fabrication

of the mounts and the testing date, the QST has to be conducted again for the mounts being used

for the baseline test as well as any new mounts fabricated.

2.3.3 Dynamic Characterization

Lastly, in order to determine the effectiveness and usability of these mounts, one must employ the concept of base excitation and displacement transmissibility. The displacement transmissibility is defined as the ratio of the displacement of a mass resting on top of the spring/damper to the displacement input base, or in our case, the mount. In order to model the transmissibility of a base-excitation problem such as the one presented in this study, the following equation is used

Where ζ is the damping ratio and ω is the frequency ratio, ω/ω_n . Plotting this displacement ratio, T_d , against the frequency ratio gives a characteristic transmissibility curve, assuming the input is sinusoidal. As is shown below in figure 2-20, a typical plot begins with a displacement transmissibility magnitude of 1 at $\omega = 1$, then the displacement transmissibility ratio increases until its peak at the resonant frequency, $\omega = 1/\sqrt{1-2\zeta^2}$, and then descends towards zero as ω increases. The peak occurs at different magnitudes depending on the damping ratio of the system. [1]

Chapter 3 | Testing Apparatus Design,

Fabrication and Methodology

This chapter is devoted to the design of experiment for this study. This chapter begins by giving a brief overview of the magnetic principles to allow the reader ease of understanding of the relationship between MR fluid and electromagnetism. Next, it highlights the equipment already in hand prior to the initiation of the study, including the pre-fabricated mounts and the electromagnetic rheometer casing designed by BM Southern. It then delves into the many modifications made to the existing apparatuses to accommodate the testing for this study as well as the parts that were designed and custom fabricated for the experiment. It then summarizes the entire physical test set-up and provides a description of the data acquisition system used for the tests. The validation process of the setup is touched on and finally the chapter ends with an overview of the design of experiment.

3.1 | Magnetic Circuitry Principles and Existing equipment

3.1.1 Magnetic Circuitry Principles

As was discussed in earlier sections, MR devices are generally operated using a powered electromagnet, a permanent magnet or a combination of the two. But an elevated wire gauge or current past a certain threshold does not guarantee an adequate magnetic field as there are other factors that influence the magnitude of the magnetic field in a device. Magnetic permeability, μ , varies from material to material ranging from highly magnetically conductive materials such as steel and iron to substances such as aluminum and air which tend to degrade magnetic field intensity, H . As common sense would dictate, materials that readily pass magnetic flux should be used to increase the efficiency of the magnetic circuit whereas having air gaps should be avoided in the flux path of an MR fluid device. If air gaps are unavoidable, then a higher number of turns or a larger current should be used to achieve the desired field.

Utilizing Kirchhoff's law in magnetic circuit form

we can view the relationship between magnetic field intensity, H , the Number of turns, N , the current, I , and the material length,

3.1.2 Existing Equipment: Electromagnetic Housings

Since this experiment was a second phase continuation of a project previously initiated by BM Southern, there were many artifacts left over from the initial static and quasi-static tests. Although some of the equipment was discarded, there were a few vital pieces that were used and adapted for the dynamic test. These items include the electromagnetic lower housing, the electromagnetic upper housing, spacer, wire wrapped coil-bobbin and two different mounts; the Rubber (RUB) and Steel (STE) core elastomeric mounts.

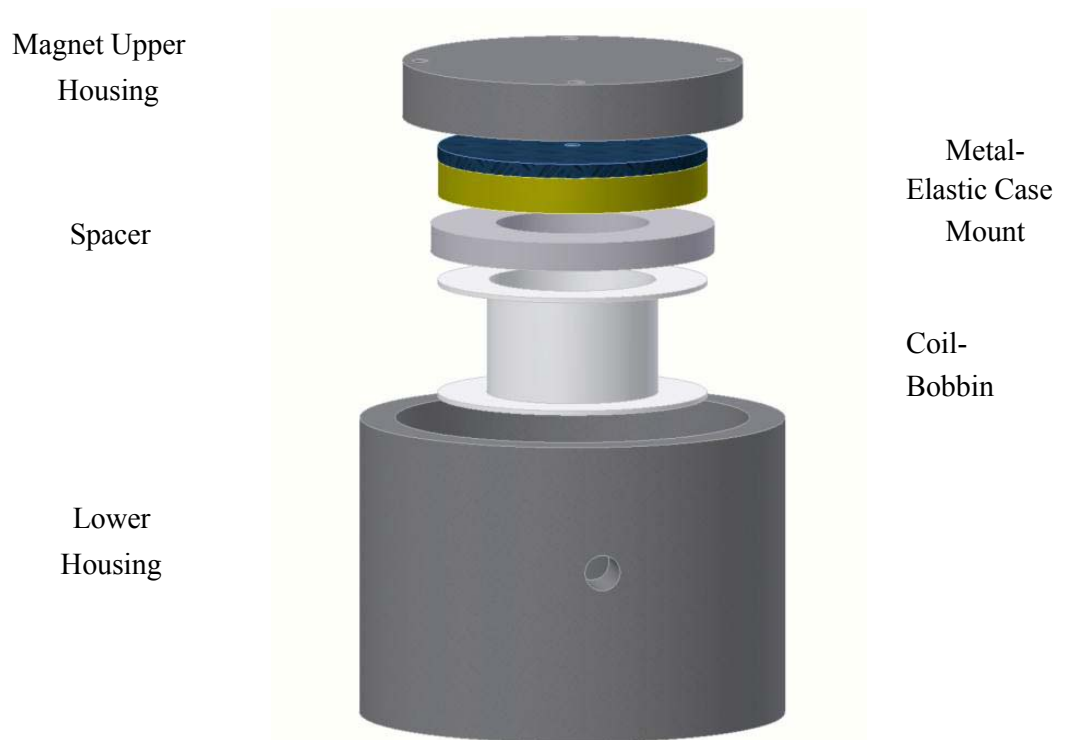


Figure 3-1: Isometric view of mount and magnetic system design, adapted from [11]

The lower housing is constructed of 304 steel and houses a core that the wire wrapped coil-bobbin fits around. It also has side walls that allow the upper housing to fit into with an air gap of 0.06 in. between its outer diameter and the inner diameter of the lower housing. In the lower housing, a spacer made of 6061 Aluminum can be put in place to prevent shock or vibrations from jarring the coil-bobbin loose from the lower housing core. The spacer also provides a flush surface for the mount to rest on. The upper housing has a flat surface with a hole in the center to fit the mount's cap-screw on the upper pole plate of the mount while keeping it flush with the surface of the upper housing. Both the upper and lower housings have threaded holes for attachment to the testing rig. The specific dimensions of the upper and lower housings are listed in Table 3-1.

Table 3-1: Dimensions and material properties for the magnetic system components as well as packaging and testing dimensions, note the difference in coil turn number, adapted from [11].

Modeled Component	Outside Diameter in.	Inside Diameter in.	Component Height in.	Material Permeability <i>B-H</i>
<u>Top-Assembly</u>				
<i>Upper Housing</i>	3.000	N/A	0.250	1018 Steel
<i>Upper-Pole Plate</i>	2.375	N/A	0.125	1018 Steel
<i>Elastomeric Casing</i>	2.375	1.625	0.3125	Air
<i>Magnetic-Pole Plate</i>	1.625	N/A	0.125	1018 Steel
<i>Fluid Cavity</i>	1.625	N/A	0.1875	MRF-140CG
<i>Spacer</i>	2.500	1.350	0.250	6061 Alu
<u>Bottom-Assembly</u>				
<i>Lower Housing Base</i>	3.750	2.400	1.800	1018 Steel
<i>Extruded Lower Housing</i>	3.750	3.125	0.8125	1018 Steel
<i>Magnetic Core</i>	1.460	N/A	1.300	1018 Steel
<i>800 Turn Electro Coil</i>	2.375	1.460	1.048	24 AWG
<i>Cosmos Coil-Bobbin 0680</i>	2.375	1.460	1.048	N/A
<u>Total-Assembly</u>				
<i>Package Dimensions</i>	3.75	N/A	2.613	
<i>Testing Setup</i>	3.75	N/A	4.613	

For the lower housing, the coil-bobbin housing had to be designed specifically to fit a coil-bobbin that would be accommodating of the magnetic needs for the experiment. However, the choice of bobbin must not interfere with the design and operation of the housings and mounts. This design can be viewed in detail in figure 3-2 below. Finally, a coil with 24 AWG copper wire at 800 turns fit into the lower housing and to provide a large value. This because with increase in current as well as time charged, electromagnets tend to drastically increase in temperature [11]. This can cause the plastic housing to melt or the copper wiring in the coil to become damaged. In order to cage the temperature, one can use a coil with a smaller number of turns. In addition, it is necessary to limit the time charged and allow time between tests for the temperature to decrease before reapplying current to the coil.

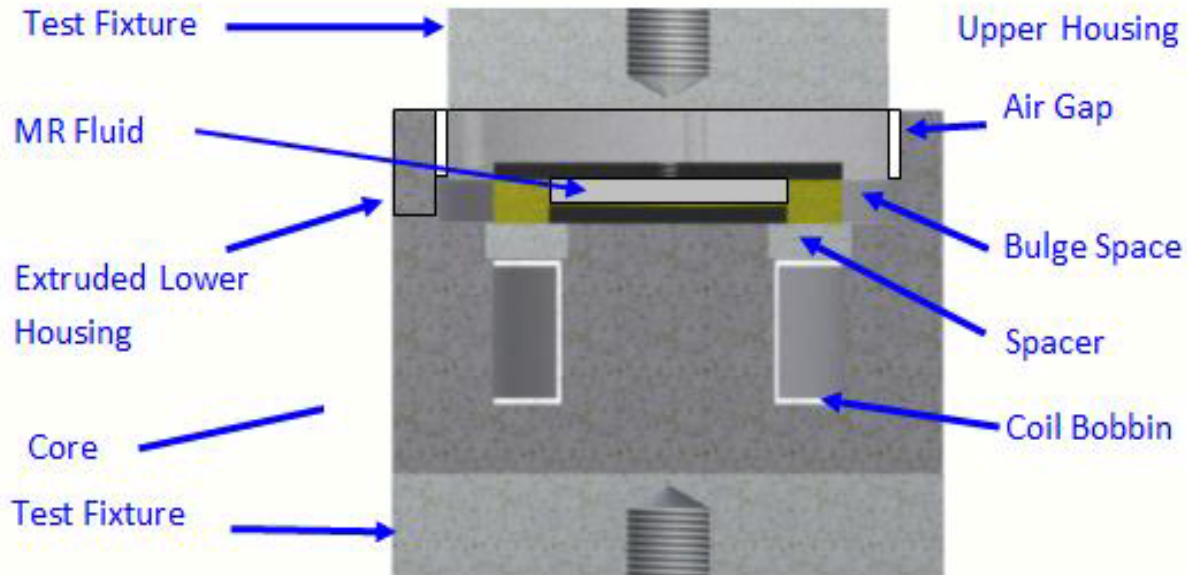


Figure 3-2: Cross-sectional view of empty metal-elastic casing and magnetic system with test fixtures, adapted from [11].

The electromagnet was powered by an Extech 100 watt switching mode DC power supply. This was chosen because of its compact size and because it allows the user to control either voltage or current. The power supply is able to produce 0.1 to 48.0 V of voltage or 0.1 to 0.1 A of current through positive and negative leads. The power supply also features a load limit in case the current applied to it is beyond its capacity, thus minimizing the possibility of shorting or blowing the circuit. This power supply, however, does not have a floating ground, which was not an issue within the scope of its use in this study [14].

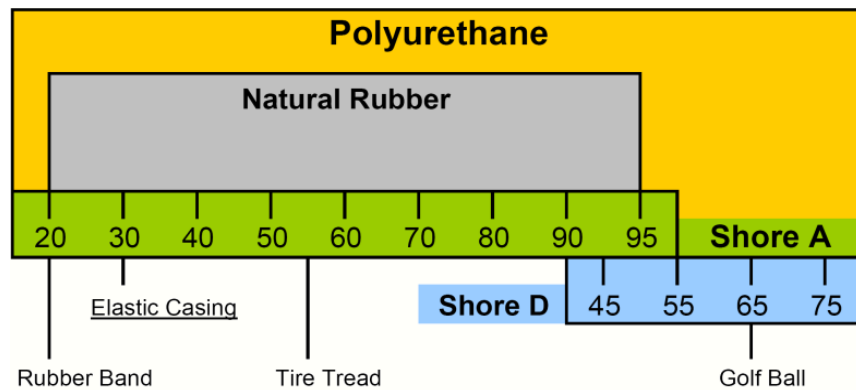
3.1.3 Existing Equipment: Pre-Fabricated Mounts

Another set of artifacts that remained from the initial study were the active and passive mounts that BM Southern had fabricated. Although many were fabricated and tested, there were only two that were actually useful for this study. The mounts that were fabricated were the results of many iterations, including active mounts filled with MR fluid as well as passive mounts with different inserts. The ones that were usable were the final versions used for the establishment of baseline properties within that study. The STE and RUB mounts would serve the same purpose in this study as well.

Specifically, a mount made entirely of rubber (RUB) and a mount made with a rubber casing and a steel insert (STE) were used. The rubber casing for all of the active and semi-active mounts in this study were made from Poly-Tek 94-30 two part polyurethane RTV mold rubber. Using the 94-30 clear combination results in a clear/amber cured color and has a Shore-A hardness rating of 30, as well as a 2000 cP mixed viscosity. This specific blend was chosen for its ease of pouring, adequate shore hardness and its clear color which allows observation of the insert and fluid cavities of the mount [19]. The table below shows a comparison of familiar items and their hardness in comparison to the TVA design's elastomeric casing.

Table 3-2:

Durometer rating comparison chart for conceptual understanding of the Shore-A hardness selected for the elastomeric casing material, adapted from [26].



All of the mounts were fabricated with identical dimensions using a three part custom machined aluminum mold. This mold has the capability of making a solid elastomeric mount, an elastomeric mount with a cavity and a metal-elastic mount with a cavity.



Figure 3-3:

Three plate mold for manufacturing elastic mounts, adapted from [11].

For the RUB mount, the standard mount dimensions shown below were used and the mold was employed with its solid single piece capabilities using only the two outer parts of the mold. Therefore, the mount that was produced is a solid two-piece mount with no cavity, as the cavity was to contain an insert of the same material [11].



Figure 3-4:

Elastic casing mounts 1.18 steel (STE), and solid 3.0 D polyurethane (RUB), adapted from [11].

In order to produce the STE mount, the 3 part mold was employed in a two-step process. Firstly, after mixing the rubber, the mold with the middle cavity plate was filled with the polyurethane, then after partly curing, the mold was opened, separated and the 1.18 Steel insert was placed inside of the cavity. Secondly, the mount was placed back in the mold with only the two outer plates and filled again with polyurethane and allowed to cure completely.

Table 3-3: Polyurethane metal-elastic and elastic casing dimensions with internal cavity dimensions for the specified insert, adapted from [11].

P.U. Casing with Type of Insert	Mount Mount Insert Insert			
	Height	Diameter	Height	Diameter
	inch	inch	inch	inch
<i>MRF</i>	0.4375	2.375	0.1875	1.725
<i>Air</i>	0.4375	2.375	0.1875	1.725
<i>3.0 D Polyurethane</i>	0.4375	2.375	0.1875	1.725
<i>1.18 Steel</i>	0.4375	2.375	0.1875	1.725

3.1.4 Existing Equipment: Roehrig Dynamic Characterization Test Rig

The equipment used for conducting the dynamic testing in this experiment was the Roehrig Electro Mechanical Actuator (K-EMA testing rig, or EMA for short). The EMA that was used as a Dynamic Characterization Tester boasts a 0.1 to 4.0 inch stroke range, which is ideal for applications with very small displacements, such as the ones in this study. The maximum velocities are in excess of 10 feet per second and output frequencies range from 0.1 Hz to over 100 Hz. The EMA also features two polished chrome parallel uprights 1 1/2 inch in diameter used for attaching a crossbar, temperature sensor and other tools and instruments. The aforementioned cross bar can be tightened to any height along the uprights. When conducting a static or quasi-static characterization test, a load cell attaches to this crossbar.



(a)



(b)

Figure 3-2: Roehrig K-EMA Set-up with bare uprights, power-supply box, and PC (a), and uprights with cross bar and load cell assembly affixed (b), adapted from [11].

The load cell used can measure a maximum force of +/- 500 lbs. (+/- 2.2 kN). The EMA also has an input board with data ports inputting information from the load cell as well as an external infra-red (IR) temperature sensor. With knowledge of the pin-out configuration and modifications to the data-card, this input can be converted to take an external input from many other types of transducers, as is discussed later in this chapter.

The EMA has a 20 hp motor output and is controlled through a desktop PC using Roehrig's proprietary Shock Absorber Dynamometer Control and Analysis Software, Shock 6.3, released in 2009. Within this software, one can design and modify a number of custom wave-forms. The user also has the option to import inputs generated in other programs or collected data converted to the proper format, given that they are within the maximum stroke range and velocity limits. The EMA is controlled by a 16-bit motion control card and is powered through a 3-phase 220 volt power supply. These features make it the ideal tool for conducting our dynamic characterization test [27].

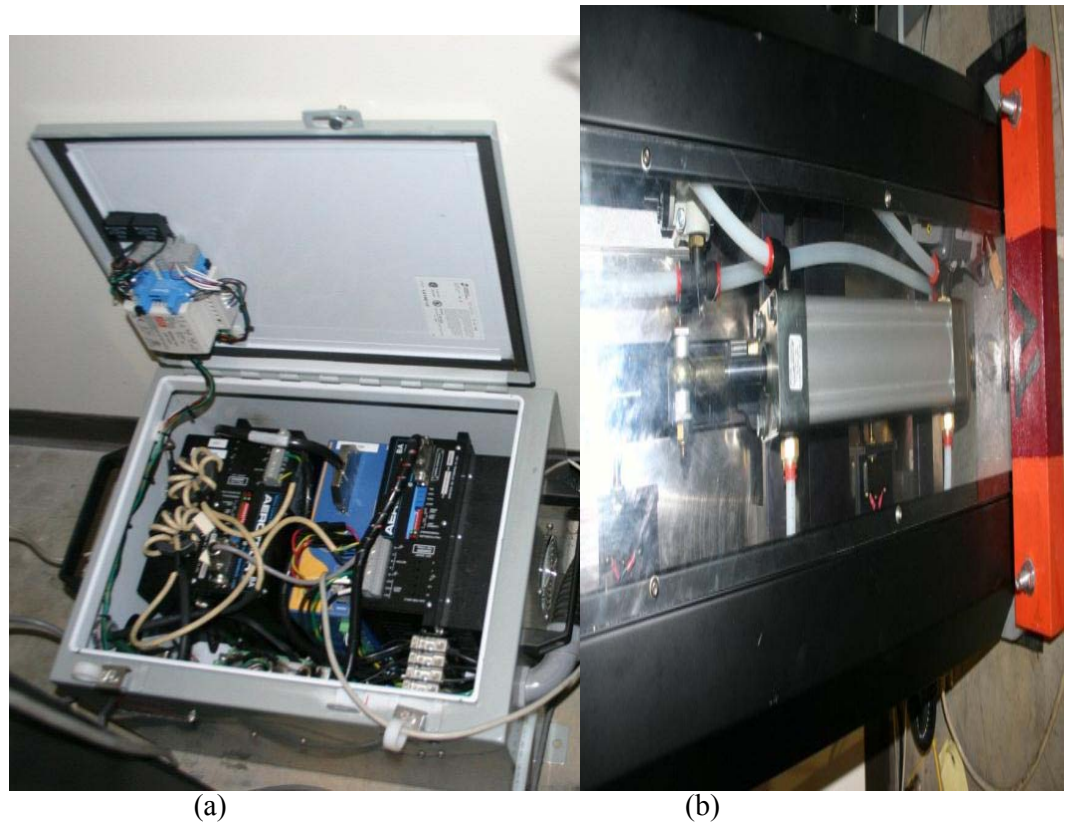


Figure 3-6: Components of the Roehrig EMA (a) open power-supply box, and (b) front motor .

3.2 | Modification of Existing Parts, New Parts Fabrication, and Physical Dynamic Principles

3.2.1 Fabricated Parts: Floating mass brace assembly

The most important aspect of the dynamic characterization is being able to measure an output displacement to an input displacement. This poses a problem because, although setting an input is as easy as programming the EMA, having a floating mass that would be placed overtop the mount and allowing it to vibrate freely in the vertical direction was a much more difficult task. This required a slight modification of the standard Roehrig EMA set up.

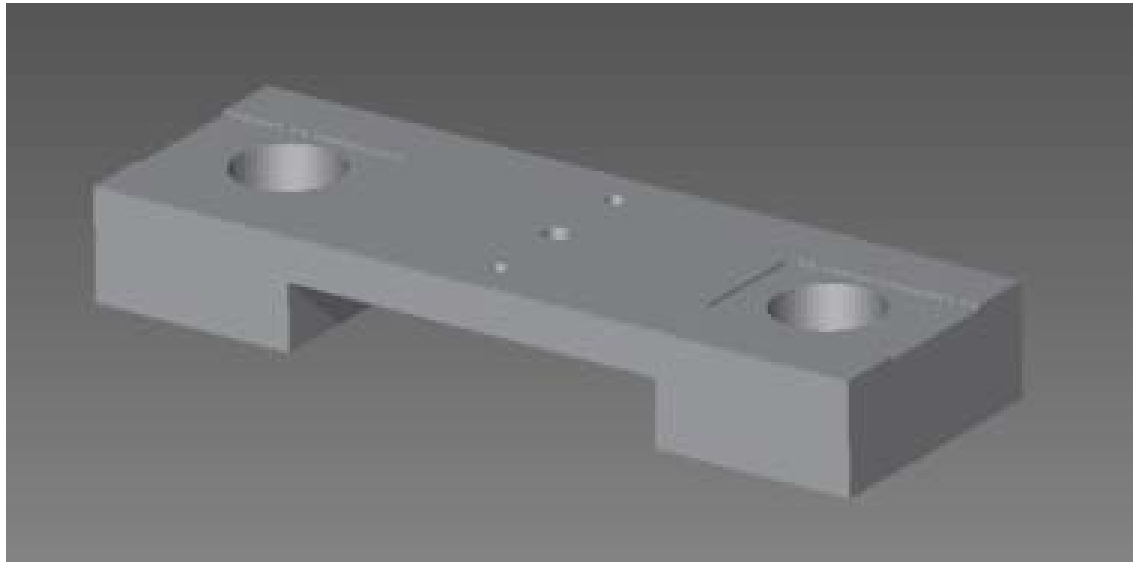


Figure 3-7: CAD Drawing of brace (top) and machined brace with bearings insert (bottom).

A brace assembly was designed to run along the existing $\frac{1}{2}$ inch diameter uprights of the EMA using INA KBZ ϵ self-lubricating sealed linear bearings [14]. These linear bearings fit

into precisely machined holes on the braces. The upper housing of the electromagnet attaches to the braces using the same size bolts that it would use to attach to the crossbar on the EMA.

Having a second brace also allows the mass plates, each ~ 1 lbs, to be tightened between the two. Two threaded upright rods were attached using bolts and washers and are then threaded through holes on either plate. The system would be experiencing input amplitudes of up to 0.5 inches peak to peak and frequencies of up to 1 Hz, so this was a necessary measure because it served the purpose of securing the required mass in place and keeping it from being thrown off during a test run. For experimental continuity, spacers were designed to fit in the space between the threaded upright rods and the holes in the mass plates. These spacers were machined to the exact diameters of the mass plates' holes thus maintaining their centered position throughout the entirety of the dynamic tests.

Each floating mass brace weighs approximately 19.5 lbs. and that weight, along with the mass of the upper magnetic housing and load cell, was then supplemented with the appropriate number of 1 lb mass plates to meet the pre-load weight requirements for each experiment respectively.



Figure 3-8: Machined Aluminum spacers (left) mass plates with pre-existing holes (right) and spacers placed inside the weights (bottom).

3.2.2 Acquired Parts: External LVDT

As was mentioned in the dynamic principles section of chapter 3, in order to determine the transmissibility ratio for the mounts being tested in this study, one needs to be able to measure the input vibration and compare it to the output of the floating mass. Although the input vibration is automatically measured through the EMA's internal linear variable differential transducer (LVDT), the vibration of the mass on the upper portion of the assembly is not. That is why an external LVDT was employed to fill that need. For this study, a Macros Sensors DC 100-2000 model LVDT was implemented. With its full scale output of 0-10V DC as well as a noise and ripple rating of < 10 mV rms, its resolution and signal to noise ratio was much more than was required as the minimum displacement required to be measured was ~ 0.1 inches peak-peak. This model has a usable range of 2.00 inches (50 mm) which is adequate for measuring the output displacement of the upper plate [39].



Figure 3-9: LVDT Power supply (left) and multi-meter (right).

To be powered, the LVDT requires a 10V DC connection with a minimum of 20 mA current. The power supply used was a Power-One HAD 10-0.4-A. This power supply is able to produce the 10 V DC and up to 400 mA current [39]. Lastly, to monitor the voltage output of the LVDT and to determine the zero point before each run, a simple multi-meter was employed and wired into the main circuit.



Figure 3-10: LVDT mounted to upper brace using custom machined bracket.

In order to properly measure the displacement of the upper floating mass, the LVDT's magnetic through-rod had to be attached directly to the mass itself. This was done by machining a bracket that was attached to the upper brace and to which the rod would attach to. The LVDT itself also had to be attached to a fixed surface in order to accurately measure the displacement at all instances. This was done by designing a bracket that would use the existing uprights on the EMA. Using the collars that were included with the EMA, the LVDT bracket is adjustable in height and can tighten around the LVDT using a clamping screw.

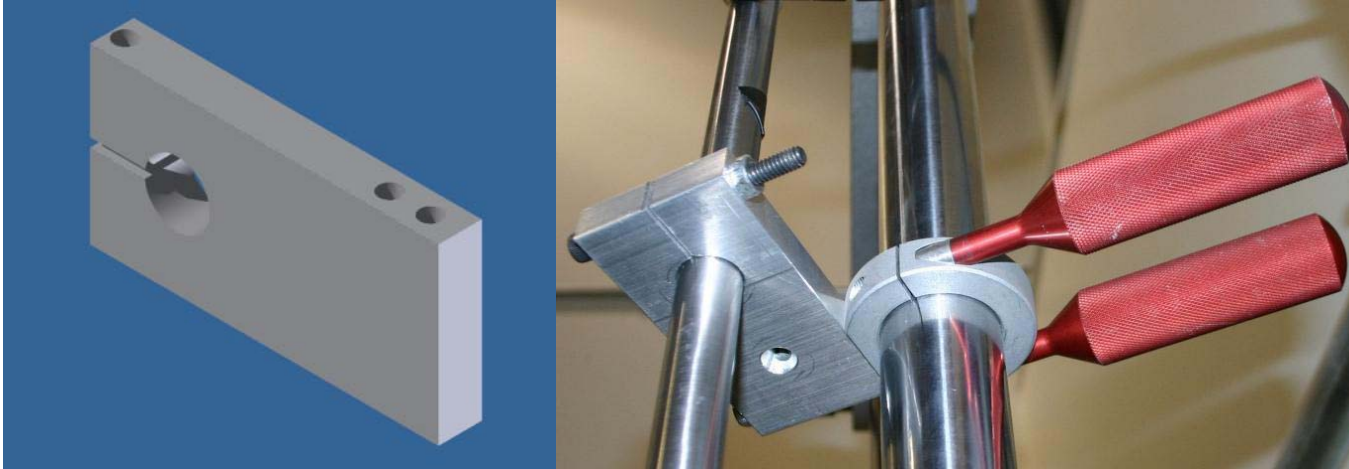


Figure 3-11: LVDT brace drawing (left) and mounted on uprights (right).

3.2.3 Modified Parts: MR Metal Elastic Mount

Lastly, due to the nature of the dynamic tests and the sometimes violent tendencies of any vibrational testing, the MR fluid mount had to be redesigned after initial failures of the design proposed by BM Southern.



Figure 3-12: Metal-elastic mount that failed under high amplitude testing.

As was shown in Table 3-4, the original MR-mount was designed to have a thickness of 0.4370 in. So, using a slightly modified version of the process BM Southern developed, a mount with a thickness increase of 20.7% and diameter increase of 4.2% was created. The mass of the mount also increased from 3.910 oz. to 4.80 oz. The insert cavity dimensions were not changed due to the fixed nature of the mold dimensions and so the amount of MR fluid still remained 0.90 oz.

Table 3-4: Original MRE dimensions and modified MRE dimensions

MRE Original	Dimensions		MRE Modified
	Inch	Inch	
Mount Height	0.4370	0.500	
Mount Diameter	2.370	2.470	
Insert Height	0.1870	0.1870	
Insert Diameter	1.720	1.720	



Figure 3-13: Original MRE mount (left) and modified MRE mount (right).

This design proved to be much more resilient and resistant to shock and vibration than the original designed which failed under the initial dynamic testing phase. The detailed instructions for fabrication of the mounts can be found in great detail in BM Southern's master's thesis [11]. The second major modification to the MR mounts that was made was the usage of a less dense MR fluid mixture. The original MRF mount was designed with MRF-1E0 mixture. Due to the lack of availability and discontinued manufacturing of that specific mixture, MRF-1Y2 was used. The fluids react differently to magnetic field application due to the drastic difference in particle density. Mainly, clumping is less likely to occur in fluids with less percentage density when operated in squeeze mode [31]. The respective B-H curves are shown below. A comparison of Finite Element Magnetic Modeling models of flux density for the original design with MRF-1E0 and the redesigned MRF mount was then conducted.

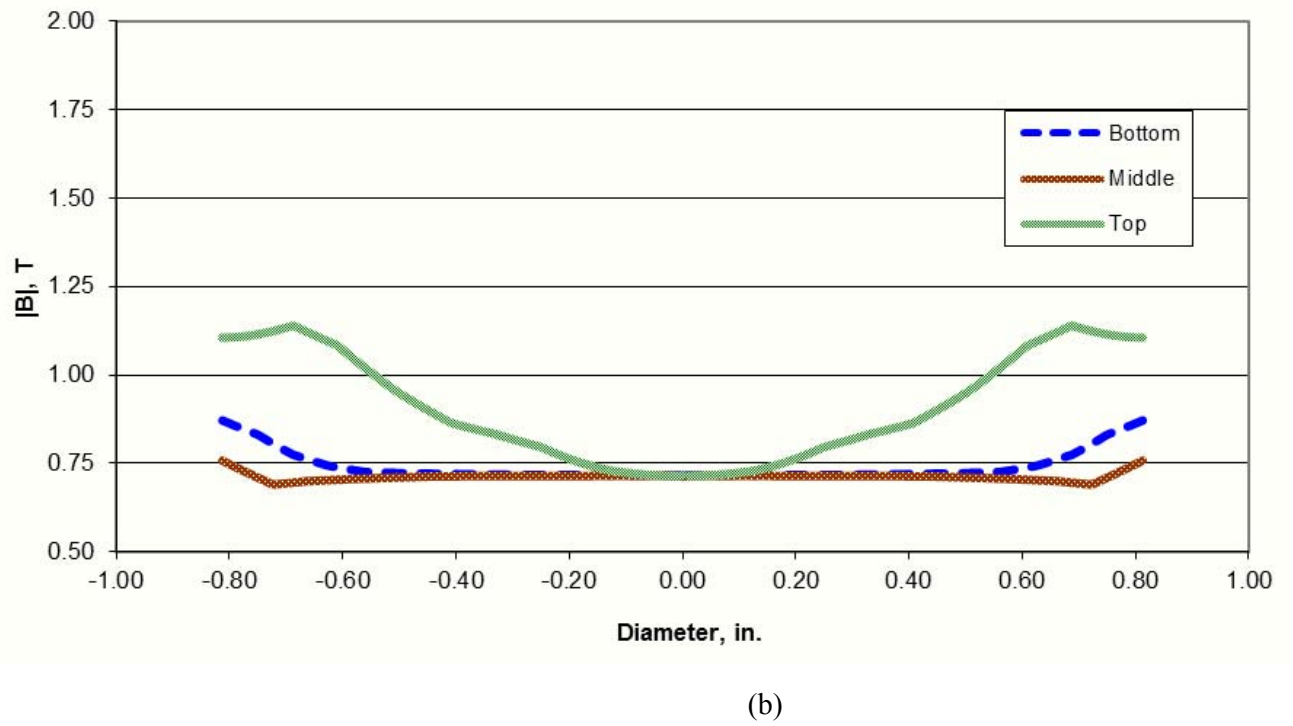
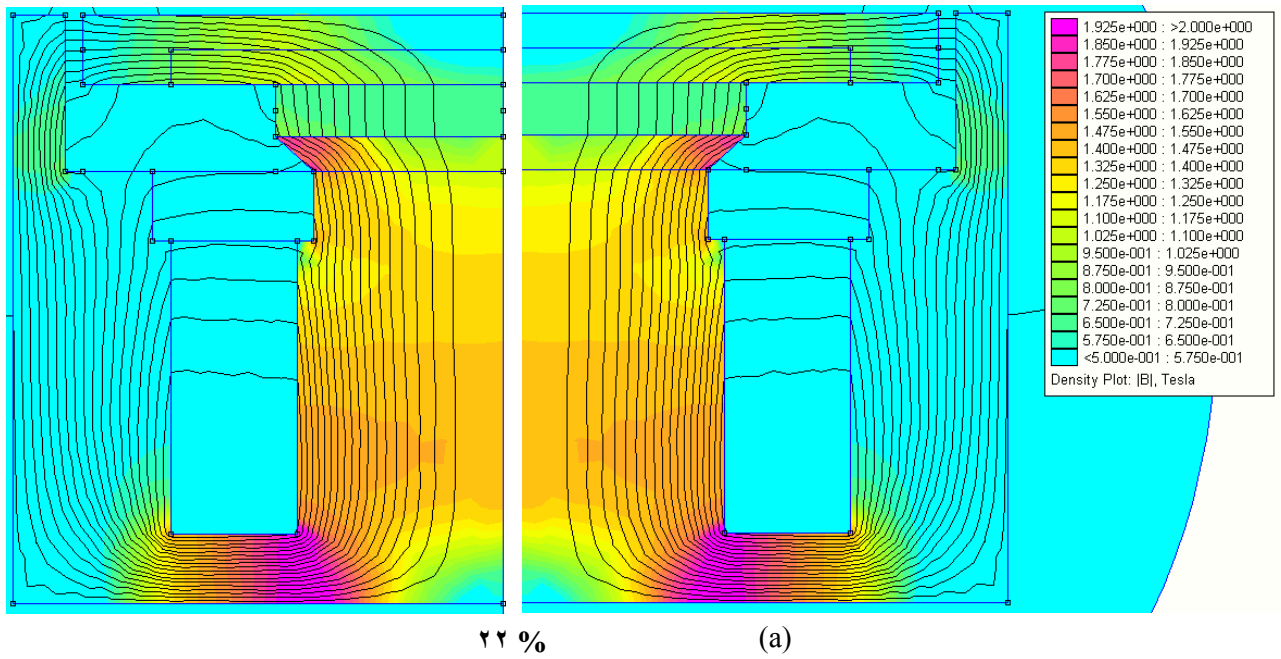
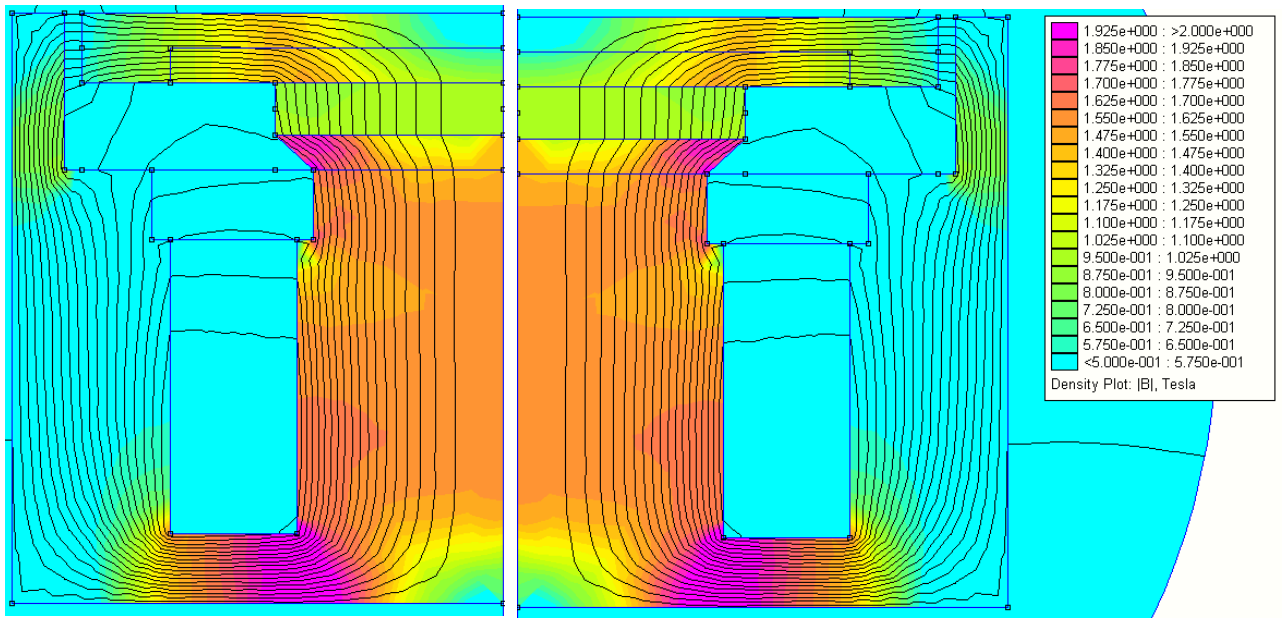
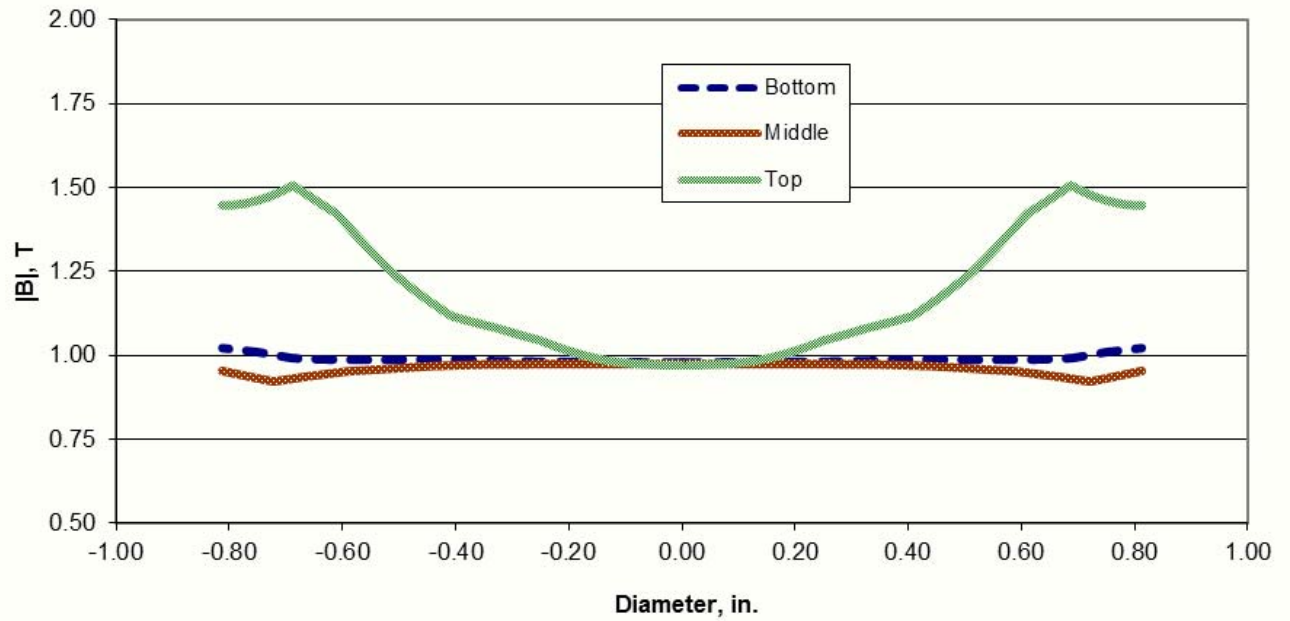


Figure 3-14: Simulated (a) Flux density for mount system and (b) magnetic flux magnitude for MRF-122 with 3 Amps of current supplied to the electro coil. adapted from [11].



(a)



(b)

Figure 3-10: Simulated (a) Flux density for mount system and (b) magnetic flux magnitude for MRF-100 with 3 Amps of current supplied to the electro coil, adapted from [11].

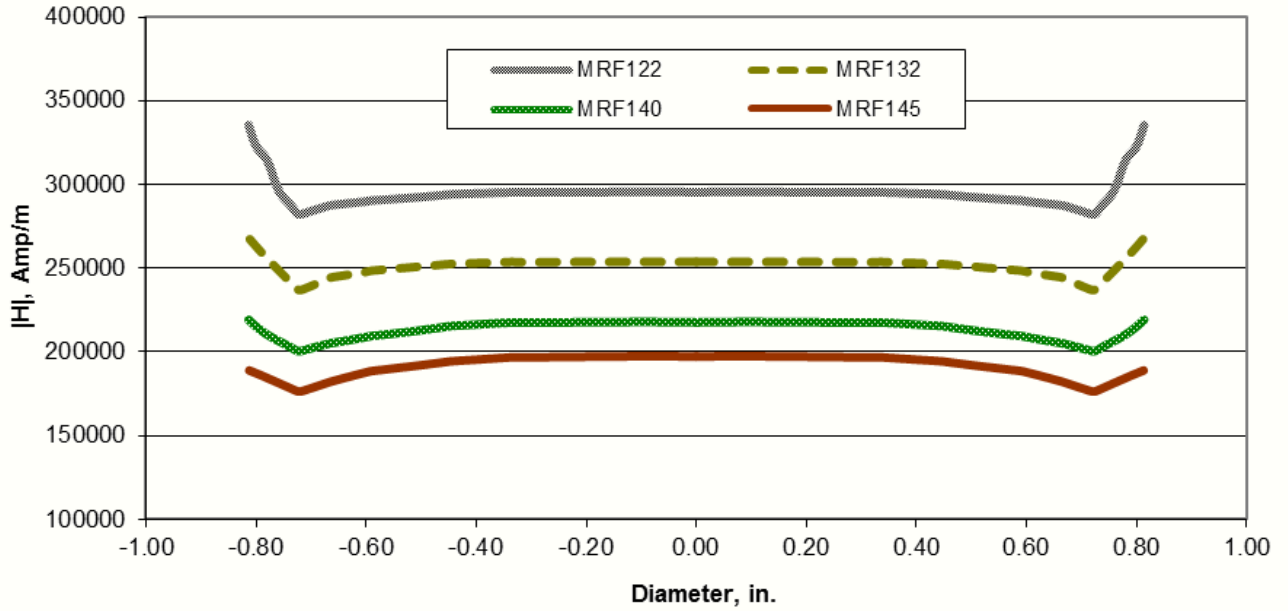


Figure 3-16: Magnitude of magnetic field intensity at the center of the fluid gap in the mount with various MR fluids including MRF-122 and MRF-140, adapted from [11].

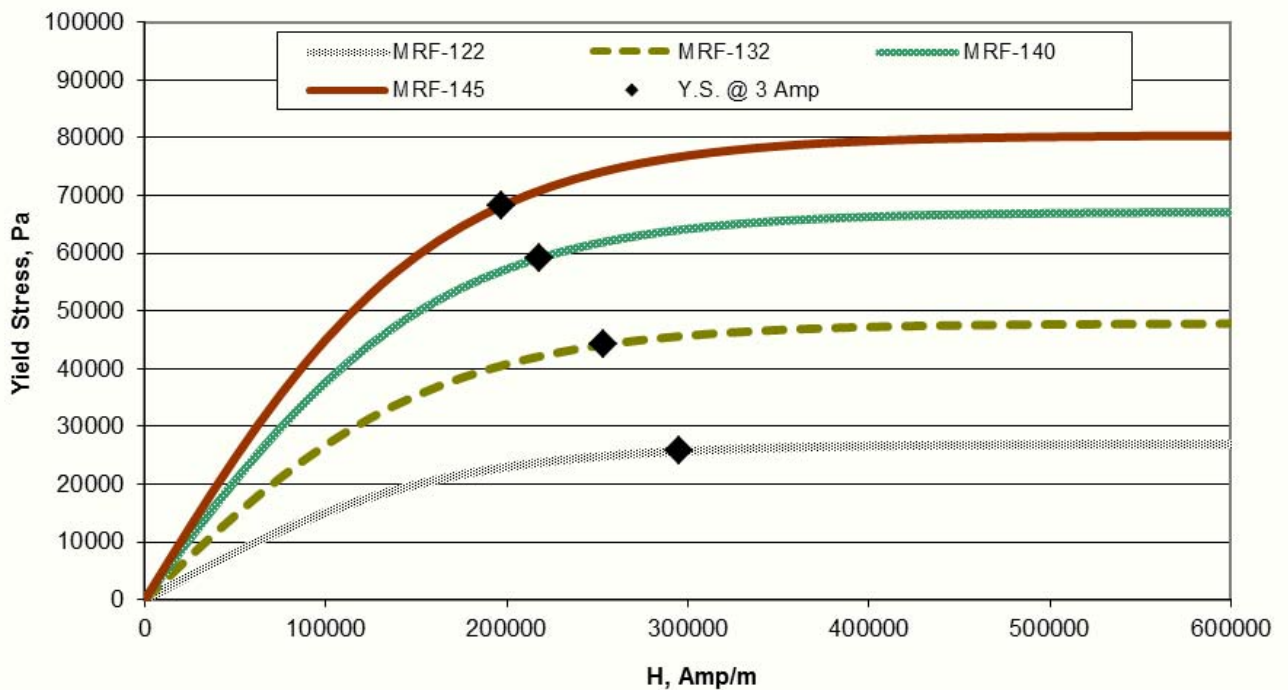


Figure 3-17: Yield stress in MR fluids marked with the maximum yield stress achieved in each fluid with various MR fluids including MRF-122 and MRF-140, adapted from [11].

3.3 | Final Experimental Set-up

3.3.1 Experimental Set-up

Using the materials and equipment discussed in the previous sections as well as the principles explained, the final experimental set-up was assembled. The assembly began with the Roehrig EMA as the base to which everything else would attach. The first step was attaching the lower electromagnetic housing to the EMA's threaded actuator rod. The upper housing of the electromagnetic assembly as well as the load-cell were then attached to the lower floating mass brace using a 1/2 inch long threaded rod and nut. The lower brace, with the threaded rods fed through the bottom, was then placed on the uprights via its linear bearings. Using a small hand-crank hydraulic lift, the upper housing was loaded with the proper amount of mass for each for the respective experiment and mount while being elevated a few inches above the lower electromagnetic housing, allowing ample space for mount insertion.

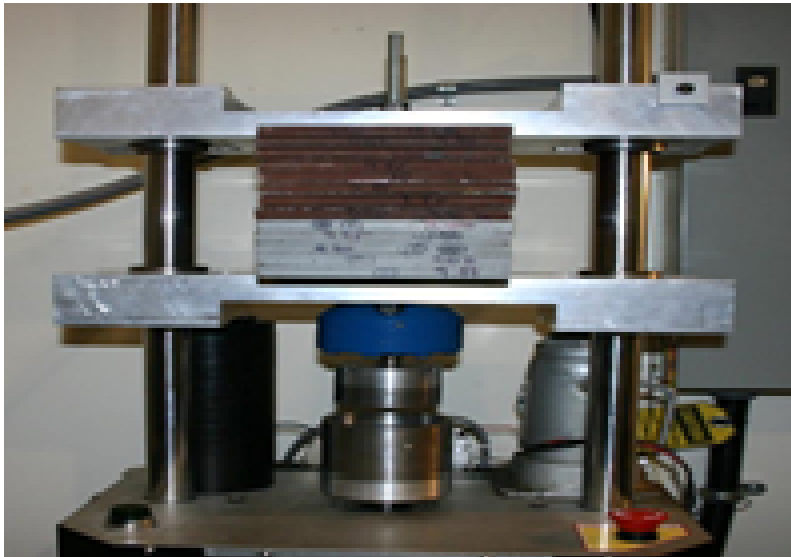


Figure 3-19: Finalized completed assembly with rheometer, load cell and weights between the braces all mounted on the EMA.

After the weights were placed on the lower brace through the threaded uprights, the spacers were fed along the threaded uprights and through the existing holes in the masses thereby centering the masses. The upper floating mass brace was then fastened with bolts and washers to the bottom brace. Lastly the LVDT was fastened to the uprights using the collar and then its

magnetic through-rod was attached to the upper assembly using the hole in the upper brace as well as the custom machined bracket. In this situation, the input force was not being measured; rather, the load cell was being used as a convenient attachment piece between the lower brace and the upper magnetic housing.

3.3.2 Data Acquisition

Most of the data acquisition for this system was simplified due to the turn-key nature of the Roehrig EMA and software combination. The input displacement, input velocity, load-cell force reading, acceleration and test specimen temperature were all measured internally through equipment provided by and validated by Roehrig Inc. However, the major problem that was encountered was the data acquisition of the floating mass displacement.

This was resolved by using the EMA's data acquisition board and the existing connection for the IR Temperature Sensor. This was advantageous for multiple reasons. The first advantage was that the Roehrig EMA board features a sampling frequency of 4000 Hz and at a maximum input frequency of 60 Hz, this is far beyond the required sampling rate for this study. Secondly, having all of the data measurement coming from one board centralizes the information into one file, thus simplifying the collection of 100's of data files. Last, and most importantly, collecting data from multiple boards creates data sets that may be inconsistent and that are asynchronous. This would require a significant amount of processing to ensure synchronization prior to the analysis of the data itself. Additionally, the board filters out known system noise from all of the sensor data in a similar fashion thus adding to the continuity of all of the measured data.



Figure 3-20:

Data acquisition board with inputs for Load Cell, Data Cable (internal), Motor Pressure (internal) and IR sensor input converted for the LVDT input.

Using the EMA's board however, was not a simple plug and play task. The first step was to make a connector that would take the proper pin designations to the EMA from the LVDT. Next, after connecting and powering the LVDT, measurements for the maximum and minimum displacement capabilities were taken using the multimeter to monitor the output voltage. After having the max and min values, the mid-point was designated as a zero value. From that datum, output voltages were measured from precise incremental displacement changes and that information was entered into the data card.

3.3.3 Set-up Validation

In order to validate the set-up of the experiment, a set of validation tests were run to ensure that the calibration and outputs were still correct. In order to begin validation, an alternate set-up had to be used. As is depicted below in figure 3-21, the linear actuator of the EMA had to be directly linked to the external LVDT. This could only be done by attaching the floating braces directly to actuator on the EMA and having the LVDT attached to the upper brace in its normal fashion. Having this setup would ensure that the LVDT is reading exactly what is being output from the EMA actuator.

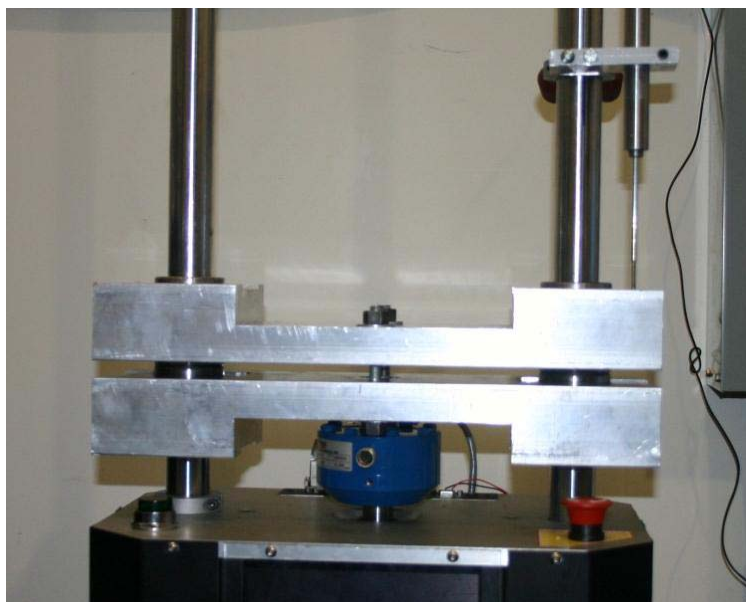


Figure 3-21: Validation set-up with direct attachment from LVDT to the actuator.

The first step of validation was to ensure that the LVDT was properly calibrated. Therefore, the calibration of the LVDT conducted in the previous section was done in multiple ways to ensure

validity. Min and max, midpoint and incremental displacement voltage output measurements were taken. The first method of incrementing the displacement was through the EMA's manual install feature, which allows the user to manually move the actuator to any desired point. Thus, having the LVDT at its determined zero point and moving the actuator in known positive and negative directions while noting the voltage outputs at each increment is an accurate way of calibration. Because the calibration and validity of the EMA's internal LVDT had to also be validated, the second form of calibration employed a similar process. However, instead of having the EMA actuator provide the displacement changes, a set of accurately machined parallel bars served the purpose of generating accurate displacements and equivalent voltage output values from the LVDT. Since the values were one and the same, they were entered into the EMA's data-card for usage as conversion factors.

Table 3-6: LVDT Displacement Values and Bit conversion values for entry into Data Card.

Displacement								
Inches	0.98	0.75	0.50	0.25	0.00	-0.25	-0.50	-0.75
Card Value								
Bits	60034	58163	49811	41460	31138	24946	16088	8243

The next step was to validate the output of the EMA. Since the values of the LVDT's measurements were validated and confirmed, the next step was to ensure that a waveform produced by the EMA was indeed the waveform that was being imported through the software. Using the same experimental set-up as the LVDT calibration, a set of simple tests were conducted using sine and triangle waves of various amplitudes. The displacement readings from the LVDT were then compared to the input waveform and the validity was assessed.